Exercise-Linked Skeletal Irisin Ameliorates Diabetes-Associated Osteoporosis by Inhibiting the Oxidative Damage–Dependent miR-150-FNDC5/Pyroptosis Axis

Jyotirmaya Behera,[1] Jessica Ison,[1] Michael J. Voor,[2,3] and Neetu Tyagi[1]

Diabetes 2022;71:2777–2792 | https://doi.org/10.2337/db21-0573

Recent evidence suggests that physical exercise (EX) promotes skeletal development. However, the impact of EX on the progression of bone loss and deterioration of mechanical strength in mice with type 2 diabetic mellitus (T2DM) remains unexplored. In the current study, we investigated the effect of EX on bone mass and mechanical quality using a diabetic mouse model. The T2DM mouse model was established with a high-fat diet with two streptozotocin injections (50 mg/kg/body wt) in C57BL/6 female mice. The diabetic mice underwent treadmill exercises (5 days/week at 7–11 m/min for 60 min/day) for 8 weeks. The data showed that diabetes upregulated miR-150 expression through oxidative stress and suppressed FNDC5/Irisin by binding to its 3′-untranslated region. The decreased level of irisin further triggers the pyroptosis response in diabetic bone tissue. EX or N-acetyl cysteine or anti–miRNA-150 transfection in T2DM mice restored FNDC5/Irisin expression and bone formation. Furthermore, EX or recombinant irisin administration prevented T2DM-Induced hyperglycemia and improved glucose intolerance in diabetic mice. Furthermore, osteoblastic knockdown of Nlrp3 silencing (*si-Nlrp3*) or pyroptosis inhibitor (Ac-YVADCMK [AYC]) treatment restores bone mineralization in diabetic mice. Micro–computed tomography scans and mechanical testing revealed that trabecular bone microarchitecture and bone mechanical properties were improved after EX in diabetic mice. Irisin, either induced by skeleton or daily EX or directly administered, prevents bone loss by mitigating inflammasome-associated pyroptosis signaling in diabetic mice. This study demonstrates that EX-induced skeletal irisin ameliorates diabetes-associated glucose intolerance and bone loss and possibly provides a mechanism of its effects on metabolic osteoporosis.

Diabetes is a group of metabolic disorders of central carbohydrate metabolism and is characterized by chronic high blood glucose levels (hyperglycemia) due to insufficient or no production of the hormone insulin (type 1 diabetes) or an ineffective response of cells to insulin (insulin resistance, type 2 diabetes mellitus [T2DM]) (1). The number of patients with diabetes has been increasing due to changes in food habits and the improvement of people's socioeconomic living standards (2). It is suggested that there are over 285 million people with T2DM worldwide (3). Its incidence is also rapidly expanding in developing and developed countries due to the high prevalence of obesity (3,4). Untreated patients with diabetes commonly develop various conditions, such as renal, neural, and cardiovascular complications, as well as bone disease, including diabetic osteoporosis (DOP) (3,5). DOP is a systemic metabolic bone disease influenced by both environmental and genetic factors and exemplified by the deterioration of bone microstructure and decreased bone mineral density (BMD) (6,7). DOP is mainly due to uncontrolled diabetic hyperglycemia and the subsequent arrest of osteoblast function with inhibiting proliferation and differentiation (8). Various studies suggest that the incidence of DOP is as high as 60% in T2DM patients (9). Therefore, there is an urgent need to understand the pathophysiological phenomena and treatment regimen for DOP.

[1]Bone Biology Laboratory, Department of Physiology, School of Medicine, University of Louisville, Louisville, KY
[2]Departments of Orthopaedic Surgery and Bioengineering, School of Medicine, University of Louisville, Louisville, KY
[3]Department of Bioengineering, Speed School of Engineering, University of Louisville, Louisville, KY

Corresponding author: Neetu Tyagi, n0tyag01@louisville.edu

Received 30 June 2021 and accepted 22 June 2022

This article contains supplementary material online at https://doi.org/10.2337/figshare.20246181.

See accompanying article, p. 2486.

Regular physical exercise (EX) is known to improve overall health status and can prevent diseases such as diabetes, obesity, age-related skeletal muscle atrophy, and osteoporosis (10,11). EX can reduce body weight, increase glucose metabolism, and prevent systemic inflammation (12,13). Several exercise models have been used to study bone mass in rodents. One study also showed that treadmill running exercise has a positive effect on cancellous bone mass and cortical bone mechanical integrity (14). In rodents, moderate exercise (through jumping, squatting, and swimming) can be shown to improve bone mass (15–17). In postmenopausal women, EX that produces mechanical stress in the bone is known to improve bone mass (18). The combined intervention of exercise and estrogen treatment promotes bone mass both in postmenopausal women and in animal models of osteoporosis (19).

miRNAs are a class of small noncoding RNAs of ~19–25 nucleotides in length that downregulate gene expression through either posttranscriptional inhibition or mRNA degradation (20,21). They especially target the mRNA of the target gene by either partial or full base pairing with the 3′-untranslated region (3′-UTR) and are involved in diverse pathophysiological processes (21). Gaur et al. (22) provided the first evidence of miRNA regulation in Dicer protein inactivation during bone metabolism. Various studies have provided evidence that miRNAs are negative modulators of osteogenesis or promote osteogenesis (23–26). However, the cross talk of miRNA and EX in DOP has remained unclear.

Pyroptosis is a programmed cell death pathway that occurs through caspase-1–mediated inflammasome activation. This leads to the release of IL-1β and IL-18 and finally causes cell swelling and rapid plasma membrane rupture (27). This newly defined programmed cell death/pyroptosis is distinct from the mechanism of apoptosis and is completely dependent on inflammatory action (28). Liu et al. (29) suggested that pyroptosis is induced in many infectious diseases. However, the mechanism behind how osteoporosis occurs in patients with diabetes with pyroptosis-mediated inflammation remains to be studied.

Thus, in the current study we investigated the hypothesis that EX can ameliorate diabetes (T2DM)-induced skeletal loss and reduce bone strength in female mice. Mechanistically, the data demonstrated that EX improved FNDC5/Irisin expression by downregulating osteoblastic miR-150-5p expression and suppressed the pyroptosis-associated proteins NLRP3, caspase-1, and gasdermin D (GSDMD) in diabetic bones. The results from the diabetic mouse model provide evidence that daily exercise may restore bone mass.

RESEARCH DESIGN AND METHODS

Animals

Six-week-old female C57BL/6J mice were obtained from The Jackson Laboratory (Bar Harbor, ME). The study protocol was approved by the Institutional Animal Care and Use Committees of the University of Louisville. All animals were maintained on a 12-h light and 12-h dark cycle. Mice were given free access to water and standard ingredient chow (solid). All mice had body weights measured weekly during the experiment.

Diabetes Induction and Dietary Intervention

At 8 weeks of age, the mice were fed either a nonfat control diet (NFD or wild-type [WT] control) or a high-fat diet (HFD) (42%) for 6 weeks. The NFD contained 10% fat, 20% protein, and 70% carbohydrates, and the HFD contained 42% fat (corn oil and lard), 28% protein, and <1% carbohydrate (D12492; Research Diets). The diabetic mouse model was established as previously described (30). For induction of T2DM in the HFD group, mice were administered streptozotocin (STZ) (Sigma-Aldrich) (50 mg/kg/body wt i.p.) every other day through or vehicle (saline) injections (total of six injections). Fourteen days later, body weight, hyperglycemia (high blood glucose levels), glucose tolerance test, and insulin and glycated hemoglobin or hemoglobin A_{1c} (HbA_{1c}) tests were performed. For study of the improvement of T2DM conditions and promotion of bone formation, the mice underwent treadmill exercises (5 days/week at 7–11 m/min for 60 min/day) for 8 weeks starting immediately following the conclusion of the course of intraperitoneal injections of STZ.

The following groups of mice were used for experimental studies: WT C57BL/6J (WT) mice, WT mice undergoing exercise (WT+EX), WT mice given HFD+STZ (T2DM), T2DM mice undergoing EX (T2DM+EX), recombinant irisin–supplemented T2DM mice (T2DM+r-irisin), antioxidant NAC–supplemented T2DM mice (T2DM+NAC), anti–miRNA-150–supplemented T2DM mice (T2DM+anti–miR-150), *si-Nlrp3* against NLRP3 inflammasome–treated T2DM mice (T2DM+siNLRP3), and pyroptotic inhibitor Ac-YVADCMK (AYC)-treated T2DM mice (T2DM+AYC).

In Vivo Administration

T2DM mice were treated with r-irisin (100 μg/kg/body wt i.p.), AYC (8 mg/kg/body wt i.p.), and NAC (75 mg/kg/body wt i.p.) three times a week for a period of 8 weeks (total 24 injections). WT control mice received normal saline through intraperitoneal injections. At the end of the treatments, animals were sacrificed and serum and bone tissues were collected.

Bone Marrow Mesenchymal Stem Cell Culture and Differentiation

Primary bone marrow mesenchymal stem cells (BMMSCs) were isolated from the experimental mice by flushing of the bone marrow (BM) of the femoral bones according to a published protocol (31,32). Cells were washed with PBS, suspended in minimum essential medium α (α-MEM), and allowed to culture in sixwell plates (Corning) in the presence of 15% heat-inactivated FBS (ATCC), 2 mmol/L L-glutamine (Invitrogen), 100 units/mL penicillin (Invitrogen), 100 mg/mL streptomycin (Invitrogen), and 50 mg/mL amphotericin B (Invitrogen). BMMSCs were grown at 37 °C

in a 5% CO_2 incubation chamber. BMMSCs were passaged at 90% confluence.

In Vitro Alkaline Phosphatase Assay and Calcium Nodule Assay

In vitro BMMSC osteogenesis was performed as per our previously described protocol (31,32). Briefly, BMMSCs were cultured using osteogenic differentiation medium (α-MEM+15% FBS supplemented with 50 μg/mL ascorbic acid, 2 mmol/L β-glycerophosphate, 100 nmol/L dexamethasone) in 12-well culture plates (Corning). On day 7 of osteogenic induction, cells were fixed with 70% ethanol for 30 min and stained with BCIP/NBT solution (Sigma-Aldrich) for 15 min. Alkaline phosphatase (ALP) activity was quantified. For in vitro calcium nodule staining, BMMSCs were fixed with 70% ethanol for 30 min on day 21 and then the cells were stained with 2% Alizarin red S (ARS) for 20 min. The images were photographed, and the calcium concentration or bone mineralized nodules was measured colorimetrically with the optical density measured at 510 nm.

Osteoclast Tartrate–Resistant Acid Phosphatase Assay and Staining

An osteoclast assay was performed as previously described (33). Briefly, BM cells were suspended in α-MEM (15% FBS) containing M-CSF (10 ng/mL) and RANKL (50 ng/mL) and were plated at 5×10^5 cells/well in 24-well culture plates. On day 5, cells were fixed in 4% paraformaldehyde and stained with tartrate-resistant acid phosphatase (TRAP) with use of a Leukocyte Acid Phosphatase kit (Sigma-Aldrich). $TRAP^+$ cells were imaged, and the total number of cells was counted. TRAP-5b activity was also measured in serum obtained from the experimental mice with an ELISA kit (no. MBS3806296; MyBioSource).

Determination of Reactive Oxygen Species Using Confocal Microscopy

For the measurement of intracellular reactive oxygen species (ROS), BMMSCs (5×10^4 cells) were cultured in osteogenic induction medium. On day 6, BMMSCs were stained with 5 μmol/L dichlorodihydrofluorescein diacetate (CM-H2DCFDA; Invitrogen) for 22 min at 37°C. For removal of the excess amount of CM-H2DCFDA dye, the cells were washed with 1× PBS and imaged under confocal microscopy. The average ROS intensity was analyzed under the various experimental conditions (34). CM-H2DCFDA is presented as a DCFDA in Fig. 2, as it is an indicator of ROS detection.

Gene Expression Using Quantitative PCR

Gene expression analysis with quantitative (q)PCR was performed per our previously published protocol (35). Total RNA was isolated from femoral BMMSCs with TRIzol Reagent (Invitrogen) according to the manufacturer's instructions. Total RNA (1 μg) from each sample was used to synthesize cDNA with an ImProm-II Reverse Transcription System kit (Promega, Madison, WI). The RT-qPCR was set up with LightCycler FastStart DNA Master SYBR Green I reagent using a Roche LightCycler 94 real-time PCR machine. The *Gapdh* gene was used as the housekeeping internal control. The gene expression is presented as a relative expression with fold change. The primer sequences of each of the gene primers are provided in Table 1.

Western Blot Analysis

Western blot analysis of protein expression was performed as in our previously described protocol (36). Following quantification of protein lysates from BMMSCs, the samples (50 μg) were loaded on an SDS-PAGE gel and electroblotted onto polyvinylidene difluoride (PVDF) membranes with use of an electrophoretic transfer apparatus (Bio-Rad Laboratories) overnight. PVDF membranes were blocked with 5% fat-free dry milk solution and incubated with primary antibodies (1:1,000 dilution, anti-FNDC5/Irisin antibody, no. ab131390; Abcam), anti-NLRP3 antibody (ab263899; Abcam); anti–caspase-1 (sc-56036; Santa Cruz Biotechnology); anti–cleaved GSDMD (50928; Cell Signaling Technology); anti–caspase-3 (sc-56053; Santa Cruz Biotechnology); anti-RUNX2 (sc-390351; Santa Cruz Biotechnology); anti-OCN (ab93876; Abcam), and anti-GAPDH 6C5 (CB1001; Merck Millipore) for 2 h at room temperature. The PVDF membranes were then incubated with secondary antibody conjugated with horseradish peroxidase (1:5,000) at room temperature for 1 h, followed by chemiluminescence detection (Clarity Max Western ECL Substrate; Bio-Rad Laboratories). The protein bands were quantitatively analyzed with an Image Lab Software system (Bio-Rad Laboratories).

Table 1—Sequences of PCR primers used for real-time qPCR and chromatin immunoprecipitation assay PCR

Gene	Primer sequences (5′→3′)
Mouse Fndc5	FP: GATGTCCTGGAGGATGAAGTGG RP: GTGGTGGTGTTCACCTCCTGAA
Mouse Runx2	FP: TTTAGGGCGCATTCCTCATC RP: TGTCCTTGTGGATTGAAAGGAC
Mouse osteocalcin	FP: GCGCTCTGTCTCTCTGACCT RP: ACCTTATTGCCCTCCTGCTT
Mouse Nfatc1	FP: GAGACAGACATCCGGAGGAGA RP: GTGGGATGTGAACACGGAAGA
Mouse cathepsin-K	FP: GGATGAAATCTCTCGCGTTT RP: GGTTATGGGCAGAGATTGCTT
Mouse Rank	FP: ACTGAGGAGGCCACCCAAGGA RP: TGAAGAGGACCAGAACGATGAG
Mouse Oc-stamp	FP: TGTAGCCTGGGCTCAGATGT RP: GTTGGTTGAGGACGTAGAGG
Mouse Gapdh	FP: TGCACCACCAACTGCTTGC RP: GGCATGGACTGTAGTCAGAG
Mouse miRNA-150	FP: GTTCAAGCAGATCATGATACTCAA RP: GTCCTGGGACAGAGCAAAGATT
Mouse U6 RNA	FP: CTCGCTTCGGCAGCACA RP: AACGCTTCACGAATTTGCGT

FP, forward primer; RP, reverse primer.

Flow Cytometry Analysis of Pyroptosis

Pyroptotic cell death was examined according to a previously published protocol (37). Briefly, the cultured BMMSCs were stained with caspase-1 antibody (D-3), FITC (sc-392736; Santa Cruz Biotechnology), and propidium iodide (PI) for 1 h and fixed with 4% paraformaldehyde on ice for 10 min. Following washing with Hanks' balanced salt solution (Sigma-Aldrich), the cells were analyzed with a BD Accuri C6 Plus cell analyzer (BD Biosciences).

Immunofluorescence

Following 7 days of osteogenic induction, the BMMSCs were fixed with 4% paraformaldehyde for 10 min. After blocking with 5% BSA for 30 min, the cells were incubated with primary antibody (anti-irisin antibody (1:500 dilution, ab131390; Abcam) overnight at 4°C. Then, the cells were incubated with secondary antibodies conjugated with anti-rabbit Alexa Fluor 488 secondary antibody (1:200 dilution; A32731; Invitrogen) for 1 h at 37°C. Finally, the BMMSCs were stained with DAPI for 10 min and imaged under a confocal laser scanning microscope (Olympus) (38).

ELISA Analysis of Bone Turnover and Inflammatory Cytokine Markers

The bone turnover markers (total procollagen type 1 N-terminal propeptide [P1NP] and C-terminal telopeptide of type I collagen [CTX]) and pyroptosis-associated cytokines (IL-1β and IL-18) were measured in the serum of experimental mice using mouse P1NP ELISA (MBS2500076), mouse CTX-1 ELISA (MBS9141384), mouse IL-1 β ELISA (ab197742), and mouse IL-18 ELISA (ab216165) kits, respectively, according to the manufacturer's instructions (39).

Measurement of Irisin and Osteocalcin With ELISA

Serum irisin levels were assessed in experimental mice with an irisin ELISA kit (cat. no. EK-067-16; Phoenix Pharmaceuticals) as previously described (40). BMMSC-derived osteocalcin levels were measured in culture media with a mouse osteocalcin ELISA kit (MBS725134; MyBioSource) as previously described. The uncarboxylated osteocalcin in serum was measured with a mouse undercarboxylated osteocalcin (ucOC) ELISA kit (MBS166078; MyBioSource) (41).

miRNA Profiling

Total RNA from the femoral BMMSCs was isolated with the miRNeasy Kit (QIAGEN, Valencia, CA). cDNA was synthesized from 200 ng total RNA with the miScript II RT Kit (QIAGEN). One microgram of the cDNA samples from each experimental group was used to amplify the differential miRNA expression with use of miScript miRNA PCR Array Mouse miFinder (MIMM-001Z; QIAGEN). The top upregulated miRNA expressions were further validated for individual miRNA expression with miScript SYBR Green PCR Kit in Roche LightCycler 94 real-time PCR machine. The relative expression level of individual miRNAs was calculated by normalization to U6 expression with the 2-ΔΔCT method. The primer sequences for individual miRNA expression are provided in Table 1.

In Silico Analysis and Prediction of miRNAs Targeted to the *Fndc5* Gene

We performed a pipeline for an in silico miRNA–mRNA interaction study using TargetScan (www.targetscan.org) miRNA prediction tools. We have predicted the potential miRNAs that target the direct binding to their 3′-UTR of the *Fndc5/Irisin* gene.

Gene Silencing and Anti-miRNA Transfection

For investigation of the functional role of *Nlrp3* in the diabetic mouse model, Nlrp3 siRNA (5′-GUGCAUUGAA GACAGGAAUTT-3′ and 5′-AUUCCUGUCUUCAAUGCAC TT-3′) or scrambled siRNA (5′-UUCUCCGAACGUGUCAC GUTT-3′) were purchased (Sigma-Aldrich) and delivered into diabetic mice with use of in vivo Lipofectamine 3.0 Reagent (IVF3001; Invitrogen) through tail vein injections three times per week at 2 μg/μL i.v. per mouse for 2 weeks (a total of six injections). Similarly, for inhibition of miR-150 expression, diabetic mice were given 2 μg i.v. synthetic anti–miR-150 (5′-CACUGGUACAAGGGUUGG GAGA-3′) or scrambled siRNA (5′-CCGAAACCUCGGUU GAUUGCGG-3′) for periods of 2 weeks by tail vein injection (Sigma) according to the manufacturer's instructions (42).

Femoral Bone–Specific Fndc5 Knockdown Through Lentiviral Particles

With mice under general anesthesia, the femoral condyles were exposed as previously described (43). With a high-speed drill with a 0.5-mm sharp steel burr (Fine Science Tools, Foster City, CA), a perforation was created in the fossa intercondyloid, through which the shRNA lentiviral particles (1.0×10^5 IFU, no. sc-145214-V; Santa Cruz Biotechnology) in 10 μL medium were injected into the distal femur region of T2DM+EX mice with a 1-mL syringe. Control shRNA lentiviral particles (sc-108080; Santa Cruz Biotechnology) were administered to the control group. Finally, the femoral hole was packed with bone wax. Mice were sacrificed at 2 weeks after surgery, and serum and femoral bones were harvested and studied for their effect on irisin expression.

Luciferase Assay

The Fndc5 3′-UTR Lenti-reporter-Luc vector was purchased (cat. no. 207240840195; ABM, Richmont, Canada). Following confluency, BMMSC culture was transfected with use of Lipofectamine 2000 (Invitrogen). After 48 h posttransfection, the cell lysates were prepared, and the luciferase activity was measured with the Dual-Luciferase Reporter Assay (Promega). The results were normalized to Renilla luciferase in the experimental groups.

Bone Resorption Assay

The bone resorption capacity of osteoclasts was determined with a bone resorption assay kit (CSR-BRA-B1; CosMo Bio Co. Ltd, Tokyo, Japan). Matured osteoclasts (1.5×10^4 cells/well) from the experimental groups were plated in fluoresceinamine-labeled chondroitin sulfate (FACS)/calcium phosphate (CaP)-coated 24-well plates. After 4 days of culture, 100 μL culture medium was collected and mixed with 50 μL resorption assay buffer in a 96-well plate. The fluorescence was measured at an excitation of 485 nm and an emission of 535 nm with a fluorometric plate reader (Tecan GENios, Salzburg, Austria). On the other hand, the 24-well cultured plate was washed with 5% sodium hypochlorite to remove the attached osteoclasts and images were taken to visualize the resorbed areas on the cultured plate under light microscopy (44).

Histology and Histomorphometry

The excised femur bones were fixed in 10% neutral buffered formalin for 48 h, followed by decalcification in 10% EDTA for 4 weeks. After decalcification, the femoral bones were embedded in paraffin and cut into 5-μm-thick coronal sections. After deparaffinizing of the sections, the samples were stained with hematoxylin-eosin solution. The femur was imaged under a light microscope at ×10 magnification and analyzed with National Institutes of Health ImageJ software. The results are shown as the number of osteoblasts per bone surface (45).

Three-Point Bending Test of Bone

The bone mechanical strength and quality were tested in femoral bone samples with a 3-point bending test (32). Briefly, the excised femoral bones were obtained from the experimental mice and stored in 1× PBS solution until testing. The 3-point bending test was performed under a load applied at a constant rate of 20 mm/min and predominantly measured the maximum load (ultimate strength) and stiffness (slope of the linear portion of the curve representing elastic deformation) of cortical femoral bone strength with use of the Bone Strength Tester TK-252C (Muromachi Kikai Co. Ltd., Tokyo, Japan).

Micro–Computed Tomography Analysis of Bone

We performed bone femoral microstructure analysis using a micro–computed tomography (micro-CT) scan as per our previously described protocol (31). The postfixed femoral bone was scanned with a SKYSCAN 1174 μ-CT scanner (Bruker, Kontich, Germany). Then, SKYSCAN Nrecon software equipped with a SKYSCAN 1174 μ-CT scanner was used to study the bone three-dimensional reconstructions. The three-dimensional images of the trabecular region of distal femurs were obtained with OsteoQuant software. The various bone morphometric parameters (trabecular bone volume/tissue volume [BV/TV] [%], trabecular number [Tb. N] [mm 1], trabecular separation [Tb. Sp] [μm], and trabecular thickness [Tb. Th] [μm]) were generated. The means of each parameter among the experimental groups are presented in the bar graph.

Statistical Analysis

All statistical analyses and graphical presentations were performed with GraphPad Prism software, v.8.2.0. All experimental data are expressed as the mean ± SEM. Significant differences between two groups were determined with a two-tailed, unpaired Student *t* test. The significant differences in more than two experimental groups were compared with one-way ANOVA in combination with Tukey multiple comparisons test. $P < 0.05$ was considered statistically significant. Experiments were repeated three times independently.

Data and Resource Availability

The data sets generated during the current study are available from the first author on reasonable request.

RESULTS

Exercise Promotes FNDC5/Irisin Levels and Improves Glucose Intolerance in Diabetic Mice

Irisin is a cleavage product of membrane-bound FNDC5 in rodents and humans, as previously described in original reports (46) (Fig. 1*A*). In the current study, using real-time qPCR, we further found that *Fndc5* expression was increased in mouse femoral BMMSCs and femoral bone tissue compared with the vastus lateralis muscle of the WT control (Fig. 1*B*). However, no difference in the expression of *Fndc5* was observed in BM cells or osteoclasts. The data also confirmed that exercise induction in WT cells (WT+EX) significantly increased *Fndc5* expression after 3 weeks of the osteogenic culture of BMMSCs compared with WT BMMSCs (Fig. 1*C*). Interestingly, the expression of *Fndc5* was improved in the T2DM+EX condition compared with the T2DM condition (Fig. 1*C*). Indeed, the *Fndc5* expression level was improved in the type IIb fibers (fast-twitch vastus lateralis muscle fibers) of the T2DM+EX condition in comparisons with the T2DM condition. However, *Fndc5* expression was higher in BMMSCs than type IIb fibers in both WT+EX and T2DM+EX conditions. However, the *Fndc5* expression level was not changed among the groups in type I fibers (slow-twitch soleus muscle fibers). With use of immunofluorescence, the data also confirmed that there was an improved expression of FNDC5 in the T2DM+EX condition compared with the T2DM condition (Fig. 1*D* and *E*). Immunoblot also showed that FNDC5 protein expression was increased in BMMSC culture lysates of the WT+EX condition compared with the WT condition, whereas FNDC5 protein expression was improved in the T2DM+EX condition compared with the T2DM condition (Fig. 1*F* and *G*). Further, the data also confirmed that femoral bone–specific stable knockdown of *Fndc5* expression (through shRNA-mediated lentiviral particles) prevents the EX-induced restoration of *Fndc5* expression in T2DM+EX+sh-irisin mice compared with T2DM+EX mice (Fig. 1*H*).

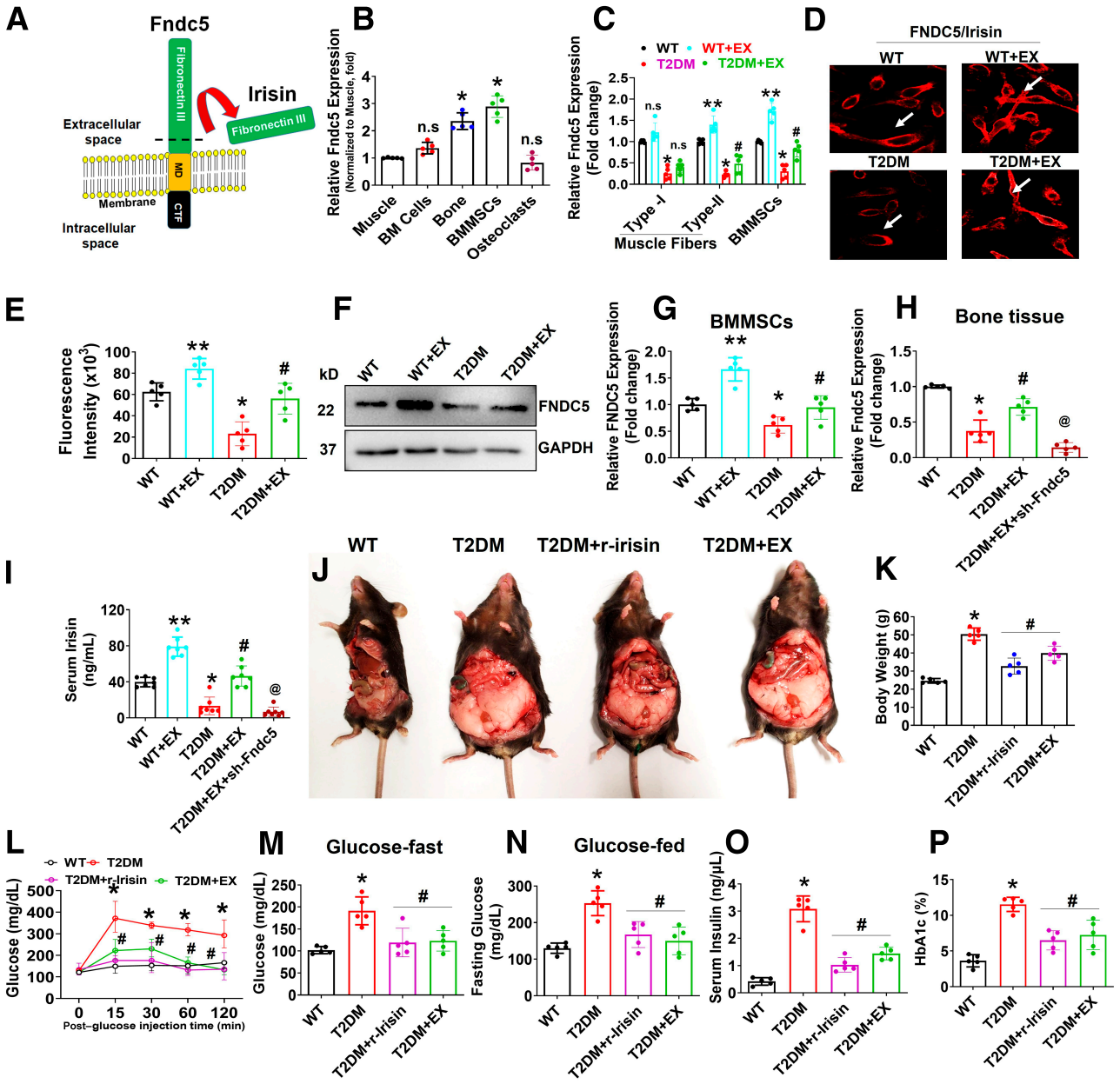

Figure 1—EX promotes FNDC5/Irisin expression in the skeleton of diabetic mice. *A*: Representative image of the structure of the myokine irisin released from the extracellular domain of the FNDC5 region of bone tissue. CTF, C-terminal fragment. *B*: mRNA transcript expression of Fndc5 in various tissues (vastus lateralis muscle, bone) and cells (BM, BMMSCs, and osteoclasts) from qPCR analysis. *C*: mRNA transcript expression of Fndc5 in slow-twitch soleus (primarily type I fibers), fast-twitch vastus lateralis (primarily type IIb fibers) muscles, and BMMSCs of the experimental mice. *D* and *E*: BMMSC expression of FNDC5 using immunofluorescence imaging (white arrow indicates membrane-bound FNDC5 expression). The bar represents the fluorescence intensity of Fndc5 expressed in BMMSCs. *F* and *G*: Protein Western blot analysis of FNDC5 in cultured BMMSCs. The bar graph illustrates the relative FNDC5 expression in BMMSCs. *H*: mRNA transcript expression of Fndc5 in femoral bone tissue. *I*: ELISA of serum irisin levels. *J* and *K*: Representative image of mice and their body weights. *L*: Glucose tolerance test in mice. *M* and *N*: Fasting glucose (*M*) and glucose levels in the fed state (*N*) in mice. *O* and *P*: Serum insulin and blood HbA_{1c} (%) levels in mice. Experiments were repeated at least three times. Data are expressed as the mean ± SEM. $n = 5$ samples per group. *$P < 0.05$ compared with the WT control; #$P < 0.05$ compared with the T2DM group; @$P < 0.05$ compared with the T2DM group. The error bars represent the SEM.

Besides, the mRNA levels of Fndc5 remained unchanged in the type IIb muscle fibers of T2DM+EX+sh-irisin mice (Supplementary Fig. 1*A*). This result indicates that femoral bone–specific stable knockdown of *Fndc5* expression was achieved without altering muscle Fndc5 expression in T2DM+EX+sh-irisin mice. Furthermore, the serum level of irisin was significantly improved in T2DM+EX mice compared with T2DM mice (Fig. 1*I*). Additionally, T2DM mice displayed higher body weight, more glucose intolerance, and increased blood concentrations of glucose, insulin, and glycated hemoglobin (HbA_{1c}) levels in comparisons with WT control mice (Fig. 1*J*–*P*). This caused hyperglycemia,

hyperinsulinemia, and intolerance to glucose. In contrast, EX or r-irisin administration prevented T2DM-induced hyperglycemia and hyperinsulinemia and improved glucose intolerance in T2DM+r-irisin or T2DM+EX mice compared with that of T2DM mice (Fig. 1*J–P*). To determine whether EX or irisin participates in the regulation of gluconeogenesis in vivo, we collected the livers of the experimental mice. Consistently, the mRNA levels of Pepck and G6pase were markedly reduced in the livers of T2DM+r-irisin and T2DM+EX mice (Supplementary Fig. 1*B*). Furthermore, the various metabolic parameters of diabetic mice under EX or r-irisin administration are presented in Table 2. This result suggests that EX improves the expression of skeletal FNDC5/Irisin and glucose intolerance in diabetic mice.

Exercise Administration Alleviated T2DM-Induced Upregulation of miR-150 by Reducing Oxidative Damage

For determination of the antioxidative function of EX in diabetes-induced oxidative damage in BMMSCs, several parameters were assessed. The total ROS, lipid oxidation product, malondialdehyde, and H_2O_2 production levels were found to be increased significantly in BMMSC cultures under T2DM conditions compared with the WT control, whereas these levels were reduced in BMMSCs under T2DM+NAC and T2DM+EX conditions compared with T2DM conditions (Fig. 2*A–D*). Concurrently, through either NAC or EX administration, the cellular antioxidant enzyme glutathione peroxidase activity was also significantly improved in both BMMSC culture extracts and BM serum under the T2DM+NAC and T2DM+EX conditions compared with the T2DM condition (Fig. 2*E* and Supplementary Fig. 1*C*).

To further identify the potent miRNAs that are differentially expressed in femoral BMMSCs in the event of diabetes-associated oxidative damage and whether EX or antioxidant NAC treatment could reverse it, we performed a qPCR-based miRNA array. The data demonstrate that several miRNAs were indeed differentially expressed in the femoral BMMSCs, as depicted in hierarchical clustering analysis (Fig. 2*F*). Indeed, the expression of two miRNAs (miR-150-5p and miR-31-5p) was concurrently upregulated in the T2DM condition compared with the WT condition (Fig. 2*F*, black arrowhead). With qPCR analysis, the expression of miRNAs (miR-150-5p, miR-31-5p) was further validated in femoral BMMSCs, and the expression of the abovementioned miRNAs was upregulated ($P < 0.0011$) in the T2DM condition. However, EX administration in the T2DM condition normalized the miRNA-150 expression ($P < 0.0001$) but not miR-31-5p (0.0605) (Fig. 2*G*). To functionally test this hypothesis, we examined miR-150-5p levels in femoral BMMSCs by stable inhibition of miR-150-5p using anti–miR-150 transfection/injection and NAC (antioxidant) treatment in T2DM mice. The data showed that anti–miR-150 and NAC treatment inhibited the expression of miR-150-5p in the T2DM+anti–miR-150 and T2DM+NAC conditions compared with the T2DM condition (Fig. 2*H*). These findings suggest that upregulation of miR-150-5p expression is oxidative damage dependent in diabetic/T2DM mice and that EX administration mitigates the above effects by reducing oxidative damage.

Exercise Reduces miR-150 Expression and Positively Regulates *Fndc5*/*Irisin* Expression

To gain insights into whether miR-150 could regulate Fndc5/Irisin expression in femoral skeletal tissue, we performed in silico TargetScan analysis. The data showed that the miR-150 sequence recognized the 1,039–1,046 bp of the conserved sequence of Fndc5 (Fig. 2*I*). To gain evidence suggesting that *Fndc5* mRNA expression is regulated by miR-150 through direct binding to their 3′-UTR regions, we performed luciferase reporter assays in vitro. We transfected BMMSCs with the *Fndc5* 3′-UTR Lenti-reporter-Luc vector for 48 h, and a luciferase assay was performed (Fig. 2*J*). The data demonstrate that there was improved luciferase activity of the reporter containing the 3′-UTR of *Fndc5* in the BMMSCs of T2DM+EX, T2DM+NAC, and T2DM+anti–miR-150 conditions compared with the T2DM condition (Fig. 2*J*). In addition, qPCR data confirmed that inhibition of the miR-150 level or EX or NAC treatment in T2DM condition significantly increased the expression of *Fndc5* in the T2DM+anti–miR-150 or T2DM+EX or T2DM+NAC compared with the T2DM group (Fig. 2*K*). These data indicated that EX significantly promotes *Fndc5* expression by inhibiting oxidative damage–dependent miR-150 function in the skeleton of diabetic mice.

Table 2—Metabolic parameters of obesity in diabetic mice

	WT	T2DM	T2DM+r-irisin	T2DM+EX
Total fat mass (g)	4.99 ± 0.11	16.72 ± 0.65*	8.11 ± 0.02#	8.04 ± 0.19#
Subcutaneous adipose tissue (% body weight)	1.75 ± 0.07	3.68 ± 0.06*	2.34 ± 0.04#	2.40 ± 0.02#
Visceral adipose tissue (% body weight)	3.20 ± 0.08	24.10 ± 0.17*	5.01 ± 0.14#	5.32 ± 0.17#
LDL/VLDL (μg/μL)	0.26 ± 0.01	0.47 ± 0.06*	0.30 ± 0.02#	0.31 ± 0.02#
HDL (μg/μL)	0.56 ± 0.03	0.34 ± 0.02*	0.47 ± 0.02#	0.50 ± 0.01#
Total cholesterol (nmol/L)	0.63 ± 0.01	0.77 ± 0.03*	0.60 ± 0.05#	0.52 ± 0.02#

The data are expressed as the means ± SEM. *$P < 0.05$ compared with the WT control, #$P < 0.05$ compared with the T2DM group.

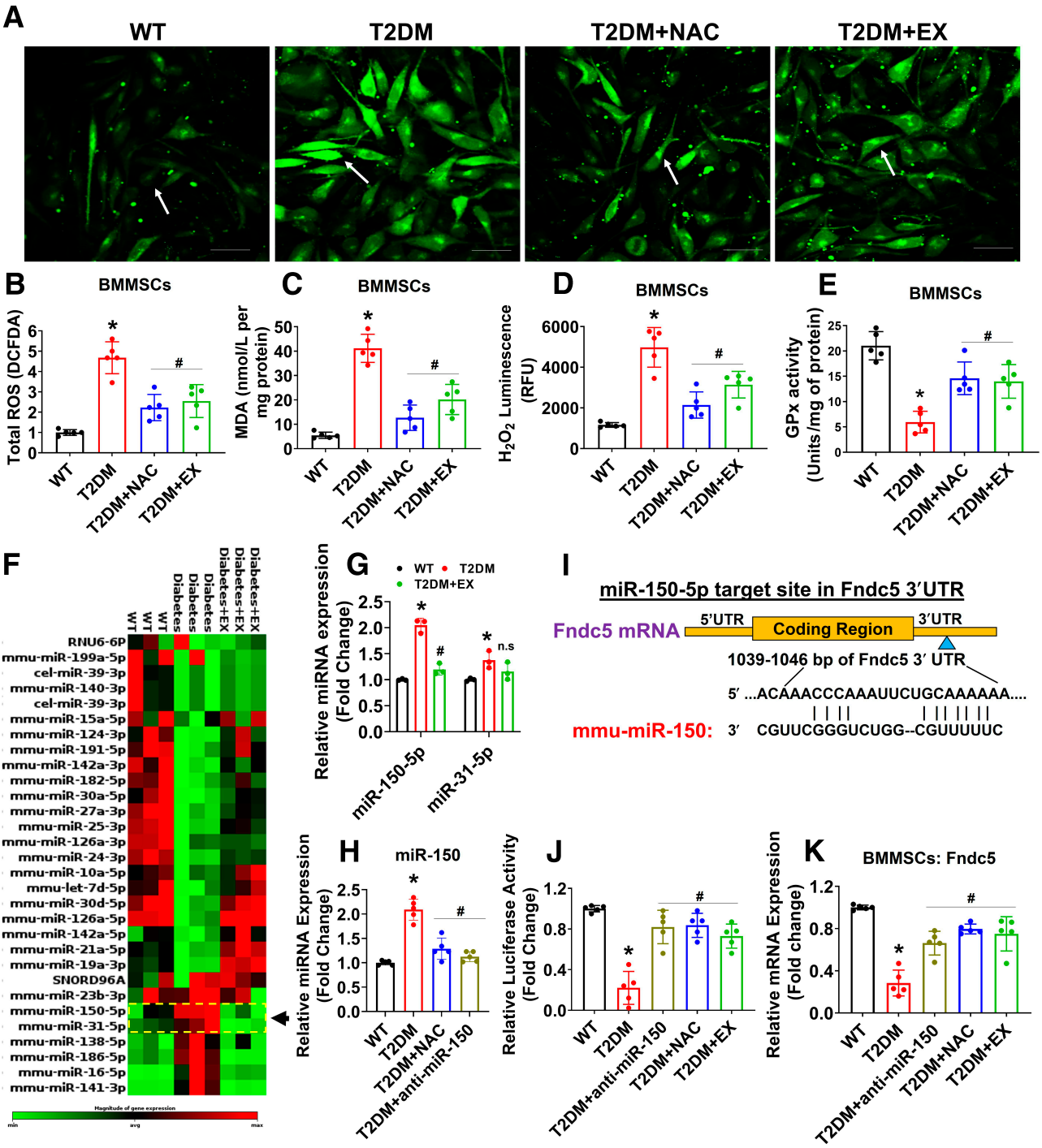

Figure 2—Exercise or recombinant irisin administration suppresses miR-150 expression by inhibiting oxidative damage in diabetic mice. *A* and *B*: Total ROS was imaged in BMMSCs using confocal microscopy. *C*: Measurement of lipid peroxidation level in BMMSCs culture. *D*: H_2O_2 production was estimated in BMMSCs culture. *E*: Glutathione peroxidase (GPx) activity was measured in BMMSCs. *F*: Heat map showing differentially expressed miRNAs in femoral BMMSCs assessed by miRNA PCR array. *G*: qPCR validation of miR-150 and miR-31-5p in BMMSCs. *H*: Effect of NAC and anti–miR-150 inhibitor on miR-150 expression in cultured BMMSCs. *I*: In silico analysis of the miR-150 binding site in the Fndc5 3′-UTR. *J*: Luciferase activity was tested in BMMSCs. *K*: qPCR analysis of Fndc5 mRNA expression. Experiments were repeated at least three times. Data are expressed as the mean ± SEM. $n = 5$ samples per group. *$P < 0.05$ compared with the WT control; #$P < 0.05$ compared with the T2DM group. The error bars represent the SEM. CM-H2DCFDA (General Oxidative Stress Indicator) is a dye to detect the ROS in cultured cells. More information can be found in *RESEARCH DESIGN AND METHODS*, but is presented here in short form, DCFDA.

Exercise or Recombinant Irisin Administration Mitigates the Central Pyroptosis Response Under Diabetes Conditions

To detect whether pyroptosis is induced in the skeleton of diabetic mice, we performed immunoblotting in extracted protein lysates from femoral BMMSCs. The results demonstrated that the expression of NLRP3, caspase 1, and gasdermin D (GSDMD) was significantly higher in T2DM BMMSCs than in WT control BMMSCs (Fig. 3*A* and *B*). However, administration of r-irisin or EX prevented the T2DM-associated changes (Fig. 3*A* and *B*). In addition, the data also demonstrated the expression of caspase-3 to verify the role of apoptosis in diabetes. The data revealed that there were no significant changes in the expression of caspase 3 among the experimental groups (Fig. 3*A* and *C*). The data also confirmed that caspase 1 activity was mitigated in BMMSC extracts of T2DM+r-irisin or T2DM+EX conditions compared with T2DM conditions (Fig. 3*D*). However, caspase 3 activity remained unchanged among the experimental conditions (Fig. 3*E*). Furthermore, we examined pyroptosis in cultured BMMSCs (caspase-1^{+} PI^{+}) using flow cytometry. The data showed that a higher proportion of pyroptotic BMMSCs (78%) was observed in the T2DM condition than in the WT control (27%), whereas the above changes were mitigated following EX or r-irisin administration in the T2DM condition (Fig. 3*F* and *G*). Additionally, pyroptotic cytokine (IL-1β and IL-18) levels were quantified with ELISA in collected serum from the experimental mice. The levels of IL-1β and IL-18 were significantly mitigated in the T2DM+anti–miR-150 condition or T2DM+r-irisin or T2DM+NAC or T2DM+EX mouse condition compared with the T2DM condition (Fig. 3*H*). These data indicate

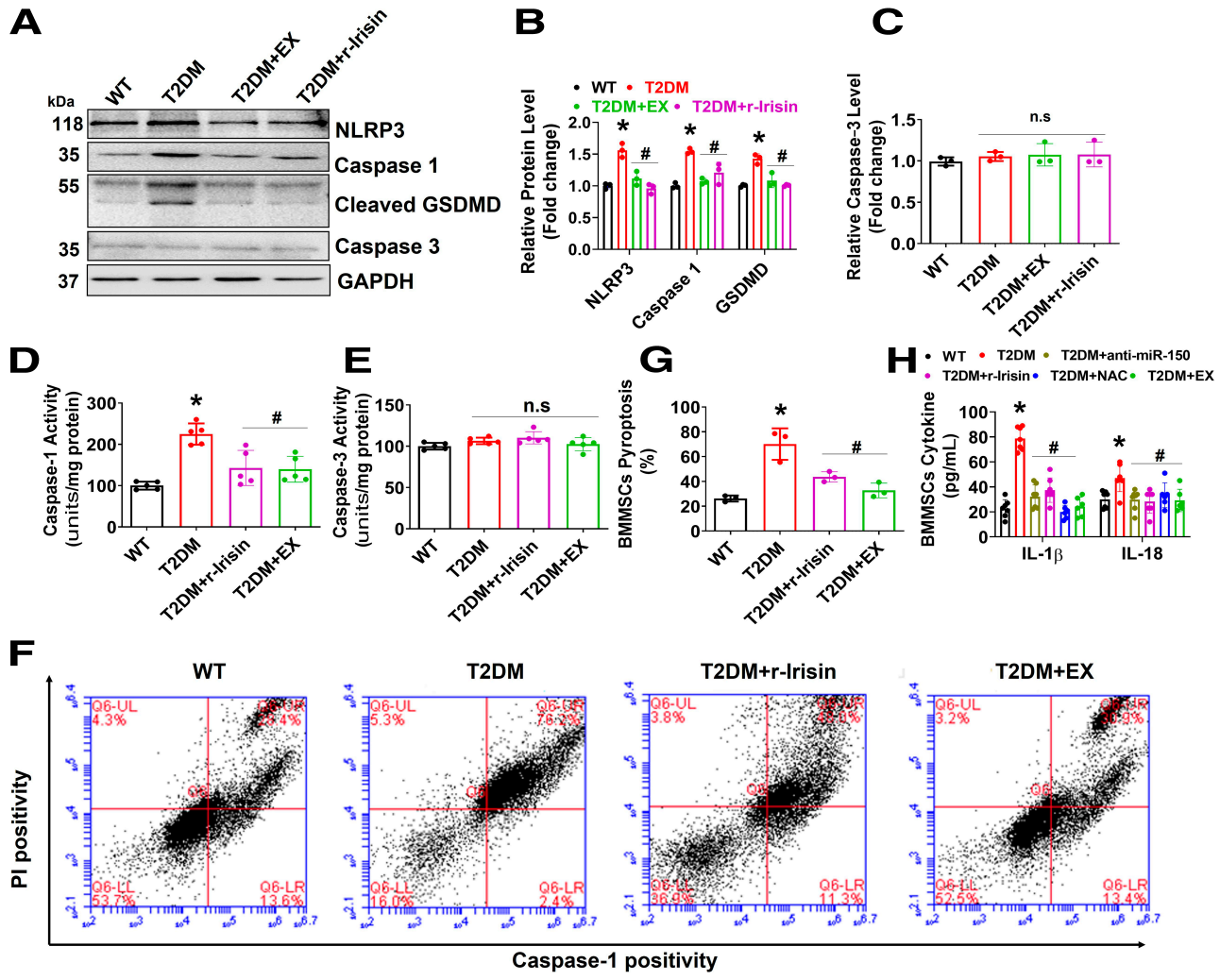

Figure 3—Exercise or pyroptosis inhibitor administration exacerbates the central pyroptosis response under diabetes conditions in vivo and in vitro. *A*: The expression of NLRP3, GSDMD, caspase-1, and caspase-3 was detected with Western blot analysis. *B* and *C*: The bar graph represents the quantification of *A*. *D* and *E*: Caspase 1 and caspase 3 activity was measured in BMMSC lysates. *F* and *G*: BMMSCs pyroptosis were tested with flow cytometry after staining with caspase 1–FITC and PI. The bar graph represents the quantification of *F*. *H*: ELISA of IL-1β and IL-18 in cultured BMMSCs. Experiments were repeated at least three times. Data are expressed as the mean ± SEM. $n = 5$ samples per group. *$P < 0.05$ compared with WT control; #$P < 0.05$ compared with the T2DM group. The error bars represent the SEM. NS, not significant.

that EX or r-irisin administration attenuates the central pyroptosis response in diabetic mice in vivo and in vitro.

Exercise or Recombinant Irisin Administration Promotes Osteogenesis by Inhibiting the Pyroptosis Mechanism

To examine whether EX has any positive effect on in vitro BMMSC proliferation capacity and osteogenesis during diabetes conditions, we cultured BMMSCs in osteogenic induction medium. The data demonstrate that BMMSC proliferation capacity (on day 3), as well as alkaline phosphatase activity (on day 7), was improved in T2DM+EX or T2DM+r-irisin BMMSC culture conditions compared with T2DM conditions (Fig. 4*A* and *B*). However, silencing irisin function through siRNA against irisin (si-irisin) prevented the EX-mediated improvement of both proliferation capacity and ALP activity in BMMSCs under T2DM+EX+si-irisin conditions compared with T2DM+EX conditions (Fig. 4*A* and *B*). Furthermore, ARS staining showed that osteogenic calcium nodule formation was improved under T2DM+r-irisin or T2DM+EX conditions compared with T2DM conditions. (Fig. 4*C*). Furthermore, osteoblastic knockdown of Nlrp3 (siRNA against NLRP3 or si-*Nlrp3*) or antioxidant NAC treatment restored bone mineralization on day 21 in vitro (Fig. 4*D*). Western blot analysis showed that EX or r-irisin administration significantly improved the osteogenic markers RUNX2 and osteocalcin (OCN) expression in BMMSCs of T2DM+r-irisin or T2DM+EX compared with T2DM BMMSCs (Fig. 4*E* and *F*). With use of a PCR assay, the data also confirmed that osteogenic marker gene (Alp, Runx2, Spp1, and Bglap) expression was improved in T2DM+EX, T2DM+r-irisin, or T2DM+NAC conditions compared with T2DM conditions (Supplementary Fig. 2*A–D*). Conversely, bone formation markers, P1NP levels, and osteocalcin were also indeed improved in T2DM+EX or T2DM+r-irisin conditions compared with T2DM conditions (Fig. 4*G* and *H*). Likewise, a significant augmentation of released osteocalcin was observed in the culture media of BMMSCs of T2DM+EX or T2DM+r-irisin conditions compared with the T2DM (Supplementary Fig. 2*E*). These results support the hypothesis that EX administration in diabetic mice augments BMMSC osteogenesis via induction of skeletal irisin and inhibition of the pyroptotic cellular response.

Exercise or Recombinant Irisin Administration Attenuates Osteoclastogenesis via a Paracrine Mechanism In Vitro

To determine whether the pyroptotic secretome (IL-1β) of diabetic BMMSCs (Fig. 3*I*) contributes to osteoclastogenesis

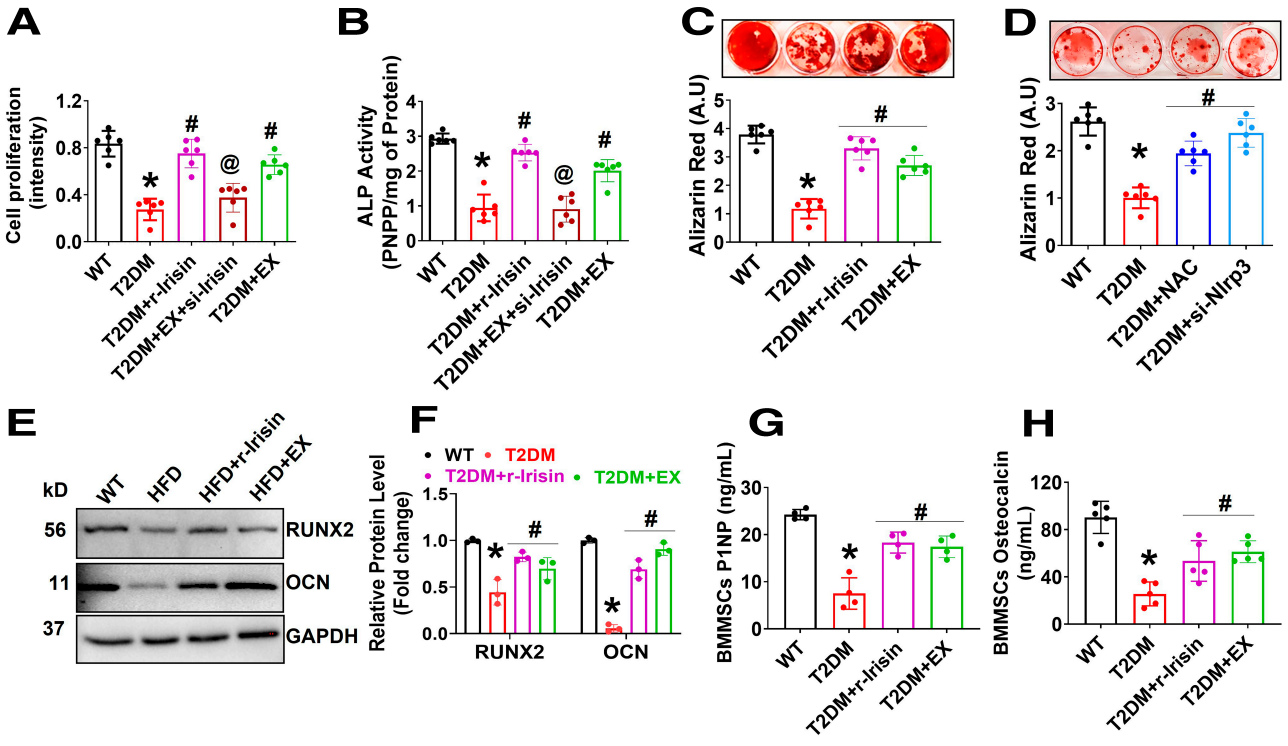

Figure 4—Exercise or direct irisin administration restores osteogenesis in diabetic mice. *A*: BMMSC proliferation was assessed by MTT assay. *B* and *C*: ALP activity (*B*) and bone calcium nodule formation assay on day 21 by ARS in BMMSC culture (*C*). *E* and *F*: Western blot analysis of the osteogenic proteins RunX2 and OCN. *G* and *H*: ELISA of the bone formation marker, P1NP level, and osteocalcin was measured in BMMSCs. Experiments were repeated three times. Data are expressed as mean ± SEM. $n = 5–6$ mice per group. *$P < 0.05$ compared with WT control; #$P < 0.05$ compared with T2DM mice; @$P < 0.05$ compared with T2DM+EX mice. The error bars represent the SEM. A.U, arbitrary units; MTT, 3-(4, 5-dimethylthiazolyl-2)-2, 5-diphenyltetrazolium bromide; PNPP, p-nitrophenyl phosphate.

and bone resorption, we performed an in vitro osteoclast TRAP$^+$ assay. Briefly, we cultured BM monocytes in conditioned medium (CM) derived from BMMSCs (Fig. 5*A*). The data demonstrated that T2DM BMMSC–derived CM (T2DM-CM) produced more mature TRAP$^+$ osteoclasts at day 4 than WT BMMSCs (WT-CM) (Fig. 5*B* and *C*). Furthermore, to study the efficacy of IL-1β in the CM of T2DM BMMSCs, we administered an IL-1β neutralizing antibody to the T2DM-CM that targets IL-1β and investigated osteoclastogenesis progression. Interestingly, the data showed that the above effects were mitigated on treatment with IL-1β antibody (T2DM-CM+IL-1β ab) compared with T2DM-CM. Additionally, mature TRAP$^+$ osteoclasts were also mitigated in T2DM+anti–miR-150-CM or T2DM+EX-CM compared with T2DM-CM conditions (Fig. 5*B* and *C*). Furthermore, TRAP-5b activity was reduced in the extracts of osteoclast cultures of T2DM+IL-1β ab, T2DM+anti–miR-150, and T2DM+EX conditions compared with T2DM conditions (Fig. 5*D*). In addition, osteoclastic gene (Nfatc1, Ctsk, Rank, and Oc-Stamp) expression was found to be downregulated in osteoclast cultures of T2DM-CM+IL-1β ab or T2DM+EX-CM conditions in comparison with T2DM conditions (Fig. 5*E* and *F*). These results indicate that the diabetes-associated pyroptotic response increases IL-1β in the BMMSC secretome and is found to activate osteoclastogenesis via paracrine-dependent action. Furthermore, in vitro bone-resorbing osteoclast activity was examined under various experimental conditions (Fig. 5*G–I*). Indeed, the data demonstrate that the T2DM condition increased the fluorescence intensity of the CM (Fig. 5*H*) from differentiated osteoclasts in FACS/CaP-coated plates and the pit formation area

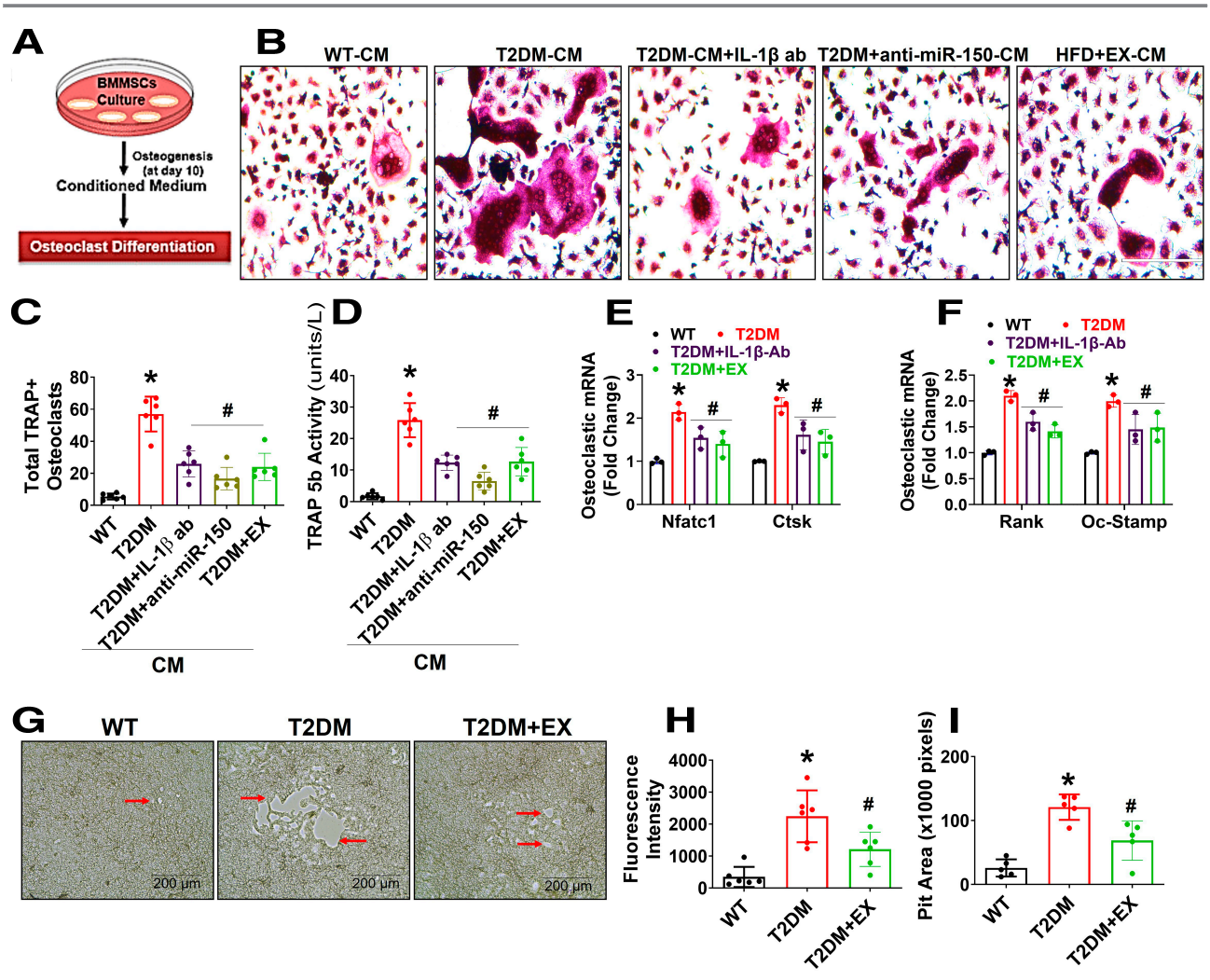

Figure 5—Exercise or neutralizing antibodies against pyroptosis attenuate osteoclastogenesis via a paracrine mechanism in vitro. *A*: Experimental strategy for the in vitro induction of osteoclastogenesis following CM treatment derived from BMMSC culture. *B* and *C*: TRAP staining of mature osteoclasts at day 4. The bar graph represents the total number of TRAP^1 osteoclasts. *D*: ELISA of TRAP-5b activity was measured in osteoclastic lysates. *E* and *F*: qPCR analysis of osteoclastic genes (Nfatc1, Ctsk, Rank, Oc-Stamp). *G* and *I*: Phase contrast microscopy of bone resorption and pit formation in vitro. Scale bar: 200 μm. The bar graphs depict the fluorescence intensity of the conditioned medium (H) and resorption pit formation area (I). Experiments were repeated three times. Data are expressed as the mean ± SEM. $n = 5$ mice per group. *$P < 0.05$ compared with WT control; #$P < 0.05$ compared with T2DM. The error bars represent the SEM.

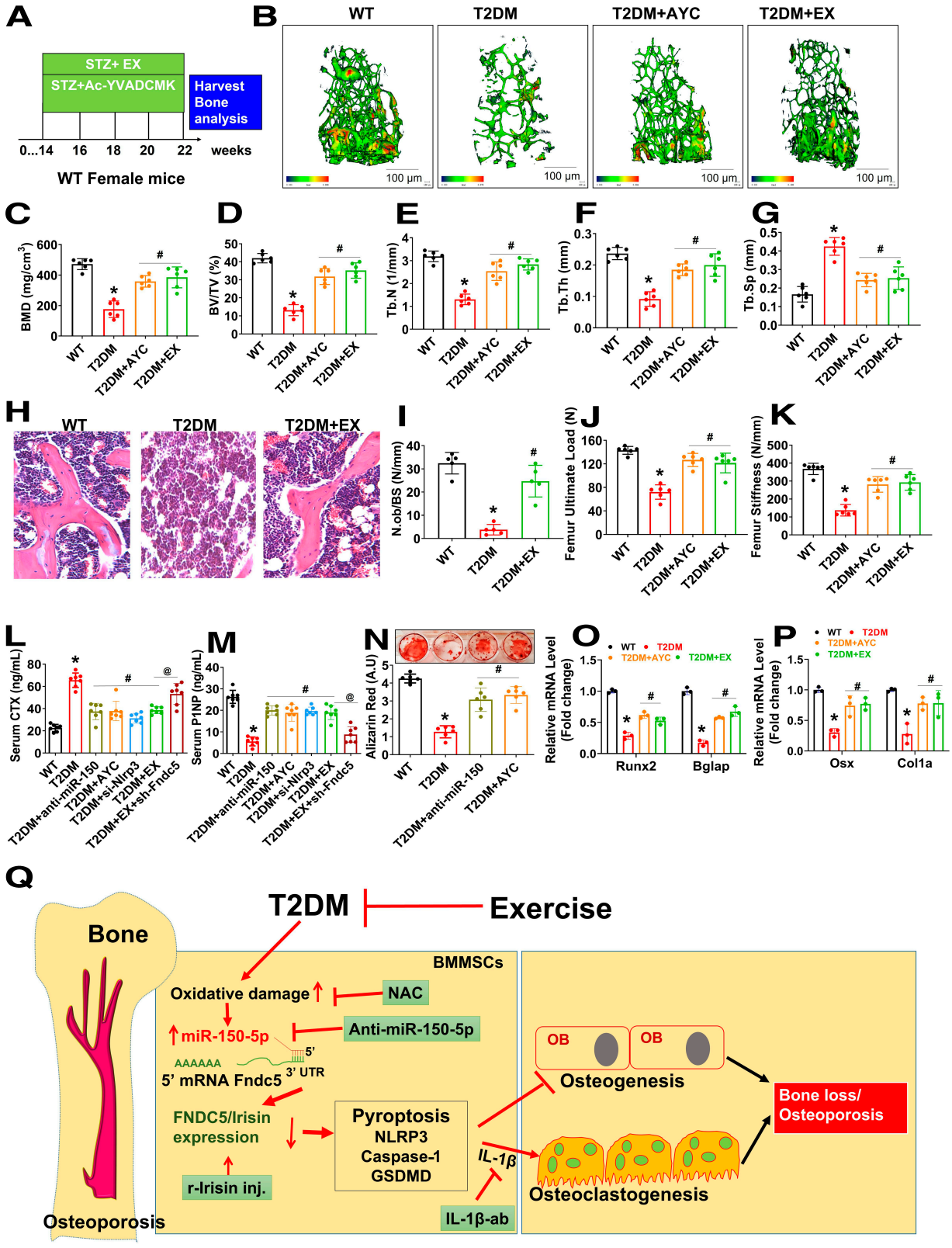

Figure 6—Exercise or miR-150 silencing restores bone mass in vivo. *A*: EX and caspase-1 inhibitor, AYC were administered independently to the experimental mice for 8 weeks. At the end of the treatment, the samples were harvested for endpoint experiments. *B*: Representative micro-CT images of distal femurs in the various experimental mice. *C*–*G*: The bone phenotype parameters BMD, BV/TV (%), Tb. N (1/mm), and Tb. Th (mm), and Tb. Sp was quantified. *H* and *I*: Hematoxylin-eosin staining of the trabecular bone volume of the femur. *J* and *K*: Femoral cortical bone mechanical quality (ultimate load (J) and stiffness (K) was tested with a 3-point bending test. *L* and *M*: Bone turnover markers (CTX (L) and P1NP (M)) were measured in the serum of experimental mice. *N*: ARS

(Fig. 5*I*) compared with the WT condition. The treatment with EX diminished the osteoclastic bone resorption activity (pit area and fluorescence intensity of the CM) compared with the T2DM condition (Fig. 5*G*–*I*).

Exercise or Pyroptosis Inhibitor Administration Mitigates Bone Loss in Diabetic Mice

For evaluation of whether diabetes (T2DM)-associated osteoporosis induced by pyroptosis and EX intervention could prevent the above effect, the diabetic mice were subjected to the EX protocol and the pyroptotic inhibitor AYC (Fig. 6*A*). Micro-CT analysis showed that femoral trabecular bone loss was increased in T2DM mice compared with WT control mice, whereas EX or AYC treatment in T2DM mice mitigated the above changes, as shown in Fig. 6*B*. Consistently, the various microarchitectural parameters of the femoral bone, such as bone mineral density, BV/TV, Tb. N, and Tb. Th, were reduced, whereas Tb. Sp was increased in T2DM mice compared with WT control mice. However, the above changes were mitigated in the femoral bone of T2DM+AYC and T2DM+EX mice compared with T2DM mice (Fig. 6*C*–*G*). To further evaluate the effect of EX on T2DM-induced bone deterioration, we performed two-dimensional histological evaluation of the mouse distal femur. The data also confirmed that the decrease in trabecular bone volume, the number of osteoblasts, and a dynamic measure of bone formation were reduced in the trabecular bone of the T2DM condition, while EX markedly enhanced the number of osteoblasts (Fig. 6*H* and *I*). Furthermore, femoral cortical bone mechanical strength (ultimate load and stiffness) was measured with a 3-point bending test. The data confirmed that EX or AYC administration increased the ultimate load and stiffness compared with the T2DM condition (Fig. 6*J* and *K*).

Furthermore, the results also showed that the P1NP level was decreased, whereas the CTX-1 level was increased, in T2DM mice compared with the WT control. However, the above changes were mitigated in T2DM+anti–miR-150, T2DM+AYC, T2DM+*si-Nlrp3*, and T2DM+EX cells (Fig. 6*L* and *M*). In contrast, silencing Fndc5 expression through the lentiviral *sh-Fndc5* approach in femoral bone prevented EX-induced production of bone remodeling markers (P1NP and CTX) in the T2DM+EX+*sh-FNDC5* condition compared with the T2DM+EX condition (Fig. 6*L* and *M*). Consistent with the reduction in osteocalcin levels in T2DM BMMSCs in vitro, shown in Fig. 4*H*, we demonstrated that the levels of ucOC in serum were improved in T2DM+EX and T2DM+r-irisin mice compared with those in T2DM mice (Supplementary Fig. 3*A*). Furthermore, serum TRAP-5b activity was significantly reduced in T2DM+anti–miR-150, T2DM+AYC, T2DM+*si-Nlrp3*, and T2DM+EX mice compared with T2DM mice (Supplementary Fig. 3*B*). In contrast, the serum levels of pyroptotic inflammatory cytokines (IL-1β and IL-18) were found to be decreased on treatment with AYC in T2DM mice (T2DM+AYC) compared with T2DM mice (Supplementary Fig. 3*C*).

Meanwhile, to further explore the role of miR-150 and pyroptosis in BMMSC osteogenesis in vitro, we treated BMMSCs with anti–miR-150 and AYC under osteogenic induction. Interestingly, the data showed that administration of anti–miR-150 and AYC improved BMMSC osteogenesis by increasing calcium nodule formation on day 21 compared with the T2DM condition (Fig. 6*N*). Similarly, osteogenic gene expression (Runx2, Bglap, Osx, and Col1a) was significantly improved in the T2DM+AYC and T2DM+EX conditions compared with the T2DM condition (Fig. 6*O* and *P*). The overall hypothesis of EX ameliorating diabetes-linked osteoporosis is depicted in Fig. 6*Q*.

DISCUSSION

The current study demonstrates several novel findings and suggests that EX prevents diabetes-mediated skeletal loss and reduces cortical mechanical strength in a mouse model by inhibiting the oxidative damage–dependent pyroptosis pathway (NLRP3, caspase-1, GSDMD) via increased expression of miR-150. To our knowledge, this is the first proof that miR-150–FNDC5/Irisin/pyroptosis signaling is governed during diabetes conditions. EX administration increased skeletal irisin expression as well as serum levels of irisin in diabetic mice. Mechanistically, diabetes upregulates miR-150 expression and suppresses Fndc5 expression, leading to activation of the pyroptosis pathway in diabetic bone tissue. Inhibition of miR-150 or r-irisin treatment in diabetic mice restores Fndc5/Irisin expression and subsequently restores bone formation. In this study we have uncovered a previously undefined novel mechanism of exercise-induced skeletal irisin ameliorating diabetes-associated bone loss via the miR-150–FNDC5/pyroptosis axis.

Results of a previous study suggested that regular exercise is required for glucose homeostasis by improving intravenous glucose tolerance and the acute insulin response to glucose, thereby protecting against postprandial hyperglycemia (47). Others have suggested that EX training protects muscle glucose metabolism and mitigates insulin resistance (48), (49). Irisin, a muscle myokine, is induced by EX and is involved in the regulation of muscular glucose uptake and the gene expression of glucose metabolism (50). However, a mechanistic understanding of exercise-induced bone-derived irisin and its role in glucose homeostasis and

staining of BMMSC cultures was measured on day 21. *O* and *P*: qPCR analysis of osteogenic marker genes (Runx2, Bglap, Osx, and Col1a). *Q*: The proposed hypothesis of EX-induced skeletal irisin prevented T2DM-induced osteoporosis through the regulation of the miR-150-FNDC5/pyroptosis axis. OB, osteoblast. Experiments were repeated three times. Data are expressed as the mean ± SEM. $n = 5$ mice per group. *$P < 0.05$ compared with the WT control, #$P < 0.05$ compared with the T2DM group.

insulin resistance has not yet been reported. A novel finding of the current study was that EX or EX-mediated bone irisin not only prevented T2DM-induced hyperglycemia and hyperinsulinemia but also improved glucose intolerance in T2DM+r-irisin or T2DM+EX mice by regulating miR-150–FNDC5/Irisin signaling.

Investigators of a recent study reported that aerobic EX was associated with a greater decline in serum glucose and HbA_{1c} (%) levels in an obese individual with T2DM and was correlated with increased osteocalcin (OCN) and uncarboxylated OCN (unOCN) (51). Mera et al. (52) demonstrated that post-EX-induced OCN signaling promotes GLUT4 translocation to the membrane and leads to glucose uptake and glycolysis in muscle fibers. In the current study, we demonstrated that EX or Irisin has a beneficial effect on the decrease in fasting glucose and HbA_{1c} (%), in part mediated through the serum level of ucOC level in T2DM condition. Further, in our study we also found that EX or irisin inhibits the expression of the hepatic gluconeogenesis genes (Pepck and G6pase) in T2DM+EX mice compared with the T2DM condition. Other have shown that OCN is essential to increase muscle mass in aging mice in part because it enhances protein translation in skeletal myotube (53). In the present study, the data demonstrated that EX or EX-linked Irisin promotes bone mineralization and bone formation through the increased production of OCN and ucOC.

Various studies have suggested that irisin has a role in bone formation or bone fracture prevention (40,54,55). Other studies have shown that circulating irisin is found to be lower than normal in patients with T2DM, which increases the risk of bone loss and fractures (40). Kim et al. (56) reported that 0.3 ng/mL irisin was detected in the plasma of 8-week-old WT mice by mass spectrometry. On the other hand, Tiano et al. (57) showed that ∼62 and ∼175 ng/mL irisin level was detected in the serum of wild-type mice using ELISA, respectively. In the current study, we found that ∼40 ng/mL irisin was detected in the serum of WT mice compared with T2DM mice using ELISA. Regarding the role of irisin in bone homeostasis, Colaianni et al. (58) demonstrated that intraperitoneal injection of r-irisin into C57 mice increased cortical bone mass and bending strength. Storlino et al. (59) suggested that r-irisin prevents osteocyte apoptosis via Atf4-dependent ERK activation in a mouse model of disuse-induced osteoporosis. In contrast, Estell et al. (60) investigated the direct role of irisin on osteoclast differentiation and bone resorption. They also showed that forced expression of the irisin precursor Fndc5 in transgenic C57 mice resulted in lower bone mass and greater in vitro osteoclastogenesis. Others have shown that irisin treatment ameliorates inflammatory bowel disease–induced bone turnover in a rodent model (61). However, the mechanisms of diabetes-associated reduction of skeletal Irisin and the subsequent activation of osteoclastogenesis and bone loss are not studied yet. In the current study, we demonstrated that the skeletal irisin level was indeed upregulated in diabetic mice after EX. Administration of r-irisin (100 μg/kg/body wt) was also found to mediate anabolic effects in bone anabolism in diabetic mice. Therefore, we conclude that EX has a strong anabolic function in bone formation in a mouse model of diabetes.

miRNAs are small, noncoding RNAs that govern distinct osteogenic functions by regulating target gene expression through binding to the 3′-UTR (62). Studies have shown that a series of miRNAs (miR-23a, miR-30c, miR-34c) inhibit osteogenesis in vitro by directly inhibiting or binding to *Runx2* (40). Other studies have shown that miR-30 family members target both *Runx2* and *Smad1* and thereby control bone mineraization (63). As miRNAs control gene expression by binding to the 3′-UTR of their target gene, we used in silico analysis through the program TargetScan to predict the target gene of miR-150-5p. We found a potential binding site in the 3′-UTR of Fndc5. Irisin is a vital component in the regulation of bone mass in diabetic mice by regulating osteoblast differentiation and mineralization. Therefore, we focused on the particular miRNAs that inhibit Fndc5 mRNA expression. However, none of the previous studies have provided evidence that miRNAs inhibit Fndc5/Irisin mRNA expression under diabetic conditions. This prompted us to understand the mechanistic basis of miRNAs that regulate osteogenic gene expression in diabetics. We demonstrated that diabetes induced miR-150-5p expression via an ROS-dependent mechanism and reduced Fndc5 expression by binding to the 3′-UTR. Furthermore, NAC administration in diabetic mice prevented ROS levels and the associated increase in miR-150 expression and restored Fndc5 expression.

Earlier studies reported that pyroptosis was induced in a host of infectious diseases, particularly those diseases caused by Gram-positive bacteria (27,64). In the current study, the murine diabetes model presented a robust ROS-dependent inflammatory pyroptotic response and bone loss. Furthermore, the expression of pyroptosis-associated proteins (caspase 1, GSDMD) was significantly induced through NLRP3 protein activation in the diabetic mouse model, along with altered bone turnover markers (P1NP and CTX) and TRAP-5b activity. However, inhibition of pyroptosis by AYC effectively prevented the diabetes-associated alteration of bone turnover markers and ameliorated diabetes-induced skeletal loss and mechanical strength in vivo. Furthermore, silencing *Nlrp3* through the siRNA approach (*si-Nlrp3*), as upstream of caspase-1, in diabetic mice significantly improved bone mineralization and bone turnover markers.

In summary, our results demonstrated that diabetes-induced miR-150-5p inhibited FNDC5 protein expression and serum irisin levels and subsequently aggravated pyroptosis-dependent skeletal loss and the inflammatory response. Inhibition of oxidative damage by NAC reduces miR-150 expression and improves irisin levels. Furthermore, inhibition of pyroptosis by AYC restored bone mineralization and bone formation activities. Importantly, EX or r-irisin also improved osteogenesis and

bone formation in diabetic mice. This result provides novel insight into the development of a promising therapeutic strategy for diabetes (T2DM)-associated bone loss.

Funding. This research study was supported, in part, by National Institutes of Health grant AR-067667 to N.T.

Duality of Interest. No potential conflicts of interest relevant to this article were reported.

Author Contributions. J.B. and N.T. conceived the ideas and designed the research. J.B. conducted the experimentation; acquired, analyzed, and interpreted data; and contributed to manuscript writing. J.I. conducted the experimentation, and M.J.V. acquired micro-CT data and analyzed data. N.T. supervised the overall manuscript. J.B. and N.T. conceived the ideas and designed the research. J.B. conducted the experimentation; acquired, analyzed, and interpreted data; and contributed to manuscript writing. J.I. conducted the western blots and biochemical experimentation, and M.J.V. acquired micro-CT data. N.T. supervised the overall manuscript. J.B. is the guarantor of this work and as such had full access to all the data in the study and takes responsibility for the integrity of the data and accuracy of the data analysis.

References

1. American Diabetes Association. Diagnosis and classification of diabetes mellitus. In Clinical Practice Recommendations. Diabetes Care 2013;36(Suppl. 1): S67–S74

2. Sami W, Ansari T, Butt NS, Hamid MRA. Effect of diet on type 2 diabetes mellitus: a review. Int J Health Sci (Qassim) 2017;11:65–71

3. Chen L, Magliano DJ, Zimmet PZ. The worldwide epidemiology of type 2 diabetes mellitus–present and future perspectives. Nat Rev Endocrinol 2011;8: 228–236

4. Forbes JM, Cooper ME. Mechanisms of diabetic complications. Physiol Rev 2013;93:137–188

5. Deshpande AD, Harris-Hayes M, Schootman M. Epidemiology of diabetes and diabetes-related complications. Phys Ther 2008;88:1254–1264

6. Hygum K, Langdahl BL, Starup-Linde J. Disentangling the association between diabetes and bone disease. Lancet Diabetes Endocrinol 2017;5:769

7. Chandran M, Tay D, Huang XF, Hao Y. The burden of inpatient care for diabetic and non-diabetic patients with osteoporotic hip fractures-does it differ? An analysis of patients recruited into a fracture liaison service in Southeast Asia. Arch Osteoporos 2018;13:27

8. Yang L, Liu J, Shan Q, Geng G, Shao P. High glucose inhibits proliferation and differentiation of osteoblast in alveolar bone by inducing pyroptosis. Biochem Biophys Res Commun 2020;522:471–478

9. Picke AK, Campbell G, Napoli N, Hofbauer LC, Rauner M. Update on the impact of type 2 diabetes mellitus on bone metabolism and material properties. Endocr Connect 2019;8:R55–R70

10. Booth FW, Roberts CK, Laye MJ. Lack of exercise is a major cause of chronic diseases. Compr Physiol 2012;2:1143–1211

11. Egan B, Zierath JR. Exercise metabolism and the molecular regulation of skeletal muscle adaptation. Cell Metab 2013;17:162–184

12. Bird SR, Hawley JA. Update on the effects of physical activity on insulin sensitivity in humans. BMJ Open Sport Exerc Med 2017;2:e000143

13. Venkatasamy VV, Pericherla S, Manthuruthil S, Mishra S, Hanno R. Effect of physical activity on insulin resistance, inflammation and oxidative stress in diabetes mellitus. J Clin Diagn Res 2013;7:1764–1766

14. Berman AG, Hinton MJ, Wallace JM. Treadmill running and targeted tibial loading differentially improve bone mass in mice. Bone Rep 2019;10:100195

15. Kodama Y, Umemura Y, Nagasawa S, et al. Exercise and mechanical loading increase periosteal bone formation and whole bone strength in C57BL/6J mice but not in C3H/Hej mice. Calcif Tissue Int 2000;66:298–306

16. Westerlind KC, Fluckey JD, Gordon SE, Kraemer WJ, Farrell PA, Turner RT. Effect of resistance exercise training on cortical and cancellous bone in mature male rats. J Appl Physiol (1985) 1998;84:459–464

17. Hart KJ, Shaw JM, Vajda E, Hegsted M, Miller SC. Swim-trained rats have greater bone mass, density, strength, and dynamics. J Appl Physiol (1985) 2001;91:1663–1668

18. Kerr D, Morton A, Dick I, Prince R. Exercise effects on bone mass in postmenopausal women are site-specific and load-dependent. J Bone Miner Res 1996;11:218–225

19. Wu J, Wang XX, Takasaki M, Ohta A, Higuchi M, Ishimi Y. Cooperative effects of exercise training and genistein administration on bone mass in ovariectomized mice. J Bone Miner Res 2001;16:1829–1836

20. Zhang L, Tang Y, Zhu X, et al. Overexpression of miR-335-5p promotes bone formation and regeneration in mice. J Bone Miner Res 2017;32: 2466–2475

21. Hu CH, Sui BD, Du FY, et al. miR-21 deficiency inhibits osteoclast function and prevents bone loss in mice. Sci Rep 2017;7:43191

22. Gaur T, Hussain S, Mudhasani R, et al. Dicer inactivation in osteoprogenitor cells compromises fetal survival and bone formation, while excision in differentiated osteoblasts increases bone mass in the adult mouse. Dev Biol 2010;340:10–21

23. Krzeszinski JY, Wei W, Huynh H, et al. miR-34a blocks osteoporosis and bone metastasis by inhibiting osteoclastogenesis and Tgif2. Nature 2014;512:431–435

24. Kim KM, Park SJ, Jung SH, et al. miR-182 is a negative regulator of osteoblast proliferation, differentiation, and skeletogenesis through targeting Fox01. J Bone Miner Res 2012;27:1669–1679

25. Li CJ, Cheng P, Liang MK, et al. microRNA-188 regulates age-related switch between osteoblast and adipocyte differentiation. J Clin Invest 2015;125: 1509–1522

26. Li H, Xie H, Liu W, et al. A novel microRNA targeting HDAC5 regulates osteoblast differentiation in mice and contributes to primary osteoporosis in humans. J Clin Invest 2009;119:3666–3677

27. Zhu X, Zhang K, Lu K, et al. Inhibition of pyroptosis attenuates *Staphylococcus aureus*-induced bone injury in traumatic osteomyelitis. Ann Transl Med 2019;7:170

28. Zu Y, Mu Y, Li Q, Zhang ST, Yan HJ. Icariin alleviates osteoarthritis by inhibiting NLRP3-mediated pyroptosis. J Orthop Surg Res 2019;14:307

29. Liu X, Zhang Z, Ruan J, et al. Inflammasome-activated gasdermin D causes pyroptosis by forming membrane pores. Nature 2016;535:153–158

30. Karasawa H, Nagata-Goto S, Takaishi K, Kumagae Y. A novel model of type 2 diabetes mellitus based on obesity induced by high-fat diet in BDF1 mice. Metabolism 2009;58:296–303

31. Behera J, Kelly KE, Voor MJ, Metreveli N, Tyagi SC, Tyagi N. Hydrogen sulfide promotes bone homeostasis by balancing inflammatory cytokine signaling in CBS-deficient mice through an epigenetic mechanism. Sci Rep 2018;8:15226

32. Behera J, George AK, Voor MJ, Tyagi SC, Tyagi N. Hydrogen sulfide epigenetically mitigates bone loss through OPG/RANKL regulation during hyperhomocysteinemia in mice. Bone 2018;114:90–108

33. Ota K, Quint P, Ruan M, et al. Sclerostin is expressed in osteoclasts from aged mice and reduces osteoclast-mediated stimulation of mineralization. J Cell Biochem 2013;114:1901–1907

34. Tyagi N, Ovechkin AV, Lominadze D, Moshal KS, Tyagi SC. Mitochondrial mechanism of microvascular endothelial cells apoptosis in hyperhomocysteinemia. J Cell Biochem 2006;98:1150–1162

35. George AK, Behera J, Kelly KE, Mondal NK, Richardson KP, Tyagi N. Exercise mitigates alcohol induced endoplasmic reticulum stress mediated cognitive impairment through ATF6-Herp signaling. Sci Rep 2018;8:5158

36. Behera J, Tyagi SC, Tyagi N. Hyperhomocysteinemia induced endothelial progenitor cells dysfunction through hyper-methylation of CBS promoter. Biochem Biophys Res Commun 2019;510:135–141

37. Liu YG, Chen JK, Zhang ZT, et al. NLRP3 inflammasome activation mediates radiation-induced pyroptosis in bone marrow-derived macrophages. Cell Death Dis 2017;8:e2579
38. Behera J, Kumar A, Voor MJ, Tyagi N. Exosomal lncRNA-H19 promotes osteogenesis and angiogenesis through mediating Angpt1/Tie2-NO signaling in CBS-heterozygous mice. Theranostics 2021;11:7715–7734
39. Greenblatt MB, Tsai JN, Wein MN. Bone turnover markers in the diagnosis and monitoring of metabolic bone disease. Clin Chem 2017;63:464–474
40. Zhang J, Valverde P, Zhu X, et al. Exercise-induced irisin in bone and systemic irisin administration reveal new regulatory mechanisms of bone metabolism. Bone Res 2017;5:16056
41. Cai P, Yan S, Lu Y, et al. Carnosol inhibits osteoclastogenesis *in vivo* and *in vitro* by blocking the RANKL-induced NF-κB signaling pathway. Mol Med Rep 2022;26:225
42. Wrobel L, Siddiqi FH, Rubinsztein DC. Transient siRNA-mediated protein knockdown in mouse followed by feeding/starving cycle and liver tissue analysis. STAR Protoc 2021;2:100500
43. James AW, Shen J, Khadarian K, et al. Lentiviral delivery of PPARγ shRNA alters the balance of osteogenesis and adipogenesis, improving bone microarchitecture. Tissue Eng Part A 2014;20:2699–2710
44. Vesprey A, Yang W. Pit assay to measure the bone resorptive activity of bone marrow-derived osteoclasts. Bio Protoc 2016;6:e1836
45. Malhan D, Muelke M, Rosch S, et al. An optimized approach to perform bone histomorphometry. Front Endocrinol (Lausanne) 2018;9:666
46. Boström P, Wu J, Jedrychowski MP, et al. A PGC1-α-dependent myokine that drives brown-fat-like development of white fat and thermogenesis. Nature 2012;481:463–468
47. Boulé NG, Weisnagel SJ, Lakka TA, et al. Effects of exercise training on glucose homeostasis: the HERITAGE Family Study. Diabetes Care 2005;28:108–114
48. Holten MK, Zacho M, Gaster M, Juel C, Wojtaszewski JF, Dela F. Strength training increases insulin-mediated glucose uptake, GLUT4 content, and insulin signaling in skeletal muscle in patients with type 2 diabetes. Diabetes 2004;53:294–305
49. Dela F, Ingersen A, Andersen NB, et al. Effects of one-legged high-intensity interval training on insulin-mediated skeletal muscle glucose homeostasis in patients with type 2 diabetes. Acta Physiol (Oxf) 2019;226:e13245
50. Huh JY, Mougios V, Kabasakalis A, et al. Exercise-induced irisin secretion is independent of age or fitness level and increased irisin may directly modulate muscle metabolism through AMPK activation. J Clin Endocrinol Metab 2014;99:E2154–E2161
51. Levinger I, Zebaze R, Jerums G, Hare DL, Selig S, Seeman E. The effect of acute exercise on undercarboxylated osteocalcin in obese men. Osteoporos Int 2011;22:1621–1626
52. Mera P, Laue K, Ferron M, et al. Osteocalcin signaling in myofibers is necessary and sufficient for optimum adaptation to exercise. Cell Metab 2016;23:1078–1092
53. Mera P, Laue K, Wei J, Berger JM, Karsenty G. Osteocalcin is necessary and sufficient to maintain muscle mass in older mice. Mol Metab 2016;5:1042–1047. DOI: 10.1016/j.molmet.2016.07.002
54. Qiao X, Nie Y, Ma Y, et al. Irisin promotes osteoblast proliferation and differentiation via activating the MAP kinase signaling pathways. Sci Rep 2016;6:18732
55. Yan J, Liu HJ, Guo WC, Yang J. Low serum concentrations of Irisin are associated with increased risk of hip fracture in Chinese older women. Joint Bone Spine 2018;85:353–358
56. Kim H, Wrann CD, Jedrychowski M, et al. Irisin mediates effects on bone and fat via αV integrin receptors. Cell 2018;175:1756–1768.e17
57. Tiano JP, Springer DA, Rane SG. SMAD3 negatively regulates serum irisin and skeletal muscle FNDC5 and peroxisome proliferator-activated receptor γ coactivator 1-α (PGC-1α) during exercise. J Biol Chem 2015; 290:7671–7684
58. Colaianni G, Cuscito C, Mongelli T, et al. The myokine irisin increases cortical bone mass. Proc Natl Acad Sci U S A 2015;112:12157–12162
59. Storlino G, Colaianni G, Sanesi L, et al. Irisin prevents disuse-induced osteocyte apoptosis. J Bone Miner Res 2020;35:766–775
60. Estell EG, Le PT, Vegting Y, et al. Irisin directly stimulates osteoclastogenesis and bone resorption in vitro and in vivo. eLife 2020;9:e58172
61. Narayanan SA, Metzger CE, Bloomfield SA, Zawieja DC. Inflammation-induced lymphatic architecture and bone turnover changes are ameliorated by irisin treatment in chronic inflammatory bowel disease. FASEB J 2018;32: 4848–4861
62. Behera J, Kelly KE, Tyagi N. Hydrogen sulfide prevents ethanol-induced ZO-1 CpG promoter hypermethylation-dependent vascular permeability via miR-218/DNMT3a axis. J Cell Physiol 2021;236:6852–6867
63. Wu T, Zhou H, Hong Y, Li J, Jiang X, Huang H. miR-30 family members negatively regulate osteoblast differentiation. J Biol Chem 2012;287:7503–7511
64. Xi H, Zhang Y, Xu Y, et al. Caspase-1 inflammasome activation mediates homocysteine-induced pyrop-apoptosis in endothelial cells. Circ Res 2016; 118:1525–1539